IOPscience iopscience.iop.org

Home Search Collections Journals About Contact us My IOPscience

Introduction of AlInAs-oxide current-confinement structure into GaInAsP/SOI hybrid Fabry–Pérot laser

This content has been downloaded from IOPscience. Please scroll down to see the full text.

2017 Jpn. J. Appl. Phys. 56 062103

(http://iopscience.iop.org/1347-4065/56/6/062103)

View the table of contents for this issue, or go to the journal homepage for more

Download details:

IP Address: 131.112.10.178
This content was downloaded on 19/07/2017 at 18:18

Please note that terms and conditions apply.

You may also be interested in:

Room-temperature continuous-wave operation of GaInAsP/InP lateral-current-injection membrane laser bonded on Si substrate
Daisuke Inoue, Jieun Lee, Kyohei Doi et al.

Thermal properties of lateral-current-injection semiconductor membrane Fabry–Perot laser under continuous-wave operation
Takuo Hiratani, Kyohei Doi, Jieun Lee et al.

Waveguide loss reduction of lateral-current-injection type GaInAsP/InP membrane Fabry–Pérot laser
Takahiro Tomiyasu, Takuo Hiratani, Daisuke Inoue et al.

Tunnel Junction for Long-Wavelength Vertical-Cavity Surface-Emitting Lasers
Shigeaki Sekiguchi, Tadayoshi Kimura, Gen Okazaki et al.

Continuous Wave Operation of Thin Film Lateral Current Injection Lasers Grown on Semi-Insulating InP Substrate
Tadashi Okumura, Hitomi Ito, Daisuke Kondo et al.

High-differential quantum efficiency operation of GaInAsP/InP membrane distributed-reflector laser on Si
Takahiro Tomiyasu, Takuo Hiratani, Daisuke Inoue et al.

Low-threshold-current operation of membrane distributed-feedback laser with surface grating bonded on Si substrate
Yuki Atsuji, Kyohei Doi, Takuo Hiratani et al.

90 °C continuous-wave operation of GaInAsP/InP membrane distributed-reflector laser on Si substrate
Takuo Hiratani, Daisuke Inoue, Takahiro Tomiyasu et al.

Japanese Journal of Applied Physics **56**, 062103 (2017)
https://doi.org/10.7567/JJAP.56.062103

REGULAR PAPER

Introduction of AlInAs-oxide current-confinement structure into GaInAsP/SOI hybrid Fabry–Pérot laser

Junichi Suzuki[1*], Yusuke Hayashi[1], Satoshi Inoue[1], Tomohiro Amemiya[1,2], Nobuhiko Nishiyama[1,2], and Shigehisa Arai[1,2]

[1]*Department of Electrical and Electronic Engineering, Tokyo Institute of Technology, Meguro, Tokyo 152-8552, Japan*
[2]*Laboratory for Future Interdisciplinary Research of Science and Technology, Tokyo Institute of Technology, Meguro, Tokyo 152-8552, Japan*

*E-mail: suzuki.j.af@m.titech.ac.jp

Received January 28, 2017; accepted April 4, 2017; published online May 30, 2017

An AlInAs-oxide current-confinement structure was introduced into a III–V/Si-on-insulator (SOI) hybrid laser for realizing an efficient light source composed of III–V/Si hybrid photonic integrated circuits. Lasing of the hybrid Fabry–Pérot laser was confirmed after introduction of the confinement structure providing both optical and electrical confinement. We determined the lasing characteristics of the designed hybrid laser, which showed a low threshold current and high external differential quantum efficiency comparable to that of conventional lasers fabricated on III–V compound semiconductor wafers. Comparison of the photoluminescence spectra of the III–V/SOI hybrid wafers before and after the process proved that oxidation had no influence on the active layer. The threshold current and external differential quantum efficiency of the fabricated laser with a stripe width of 4.5 μm and cavity length of 500 μm were obtained as 50 mA and 11%/facet, respectively.
© 2017 The Japan Society of Applied Physics

1. Introduction

Widespread use of wireless communication devices such as smartphones and tablets, and other video transmission services, has contributed to an explosive growth in the Internet traffic in recent years. Investigations have discovered that the annual global IP traffic is expected to surpass the zettabyte [ZB; 1000 exabytes (EB)] threshold in 2016, and reach 2.3 ZB by 2020.[1] Additionally, machine-to-machine communication is also undergoing an enormous increase in the data capacity owing to the rapid development of the Internet of Things and data centers owned by over-the-top service companies.[2,3]

A highly developed communication system is necessary for supporting this information era. The communication system must be able to handle the continuously increasing data capacity, the high-speed optical signals, and the low-power routing operations. The demand for flexible function routers, in particular, has increased as the dynamic computing technologies based on software-defined networks (SDNs) have been making great progress in the recent years.[4]

In this context, our research aims to realize a large-scale integrated photonic platform for one-chip routers using Si photonics, which is considered to be a better solution than the conventional packaging of bulk components used for realizing high-density integration of optical devices such as light sources and amplifiers.[5–7] Besides, the integration of many elements on-chip may reduce the total power consumption by reducing the total system power margin, as usually, surplus power is allocated to each element. Furthermore, we also proposed a reconfigurable photonic integrated circuit or the so-called photonic field-programmable gate array based on this on-chip platform.

Si photonics offers several advantages such as good transparency of Si at around 1.3–1.5 μm, compatibility with CMOS processes, and capability of providing high-density optical circuits owing to the large refractive-index difference between Si and SiO_2 in the low-cost Si-on-insulator (SOI) wafers. SOI-based waveguide-type passive devices have been reported in the recent years, such as the low-loss channel waveguides[8,9] with reduced line edge roughness and the optical modulators[10–12] or switches[13,14] operated by dynamically adjusting the refractive index. However, the indirect bandgap of Si causes difficulty in realizing active optical devices such as laser diodes or optical amplifiers, which are necessary in optical routers.[15,16]

III–V/SOI hybrid integration is considered a promising solution for enabling integration between the III–V compound semiconductor laser and the Si platform, by using bonding technologies. These types of hybrid lasers can be realized using adhesive benzocyclobutene bonding[17] or direct bonding technologies,[18,19] which are currently more attractive than the direct epitaxial growth of a III–V compound semiconductor on Si, in terms of performance, as they do not suffer from crystal lattice mismatch.

Optical modulation and signal transmissions based on integration with hybrid lasers and other optical devices were reported recently.[20,21] However, hybrid lasers are still considered inferior to the conventional lasers fabricated on III–V compound semiconductor wafers, in terms of the threshold current and external differential quantum efficiency. Conventional hybrid lasers use proton implantation[20,21] for current confinement. This method has difficulties in terms of width control, especially for narrow current-confinement widths, because of proton beam scattering.

In this paper, we focus on a current-confinement structure for improving the lasing characteristics of a hybrid laser. An AlInAs-oxide confinement structure[22] is introduced into a III–V/SOI hybrid laser for current confinement, instead of using the common proton implantation method. The lasing characteristics of the hybrid laser with AlInAs-oxide confinement structure are determined, and an oxidized III–V/SOI bonded wafer is assessed before the introduction of the confinement structure. Based on this investigation, a hybrid Fabry–Pérot laser with AlInAs current-confinement structure is fabricated, and its characteristics are discussed.

2. Estimation of lasing characteristics of hybrid lasers with AlInAs oxide

Oxide confinement structures of III–V compound semiconductors layers with Al content were vigorously developed in the 1990s, for realizing low–threshold-current operation of both in-plane lasers[23,24] and vertical-cavity surface-emitting lasers (VCSELs).[22,25]

 © 2017 The Japan Society of Applied Physics

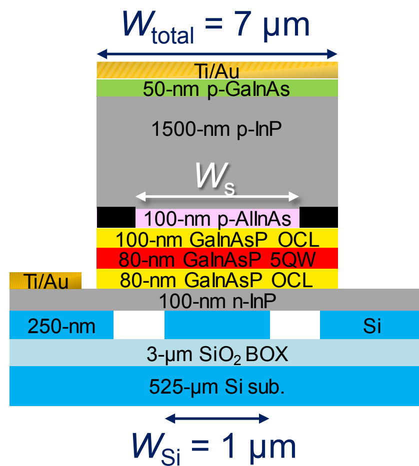

Fig. 1. (Color online) Cross-sectional view of the III–V/SOI hybrid laser used in a simulation.

Other structures such as the buried mesa stripe structure based on regrowth process[26] or polymer cladding[27] and the low-index-material sandwiching active layer with lateral current-injection structure[28] have been proposed for obtaining higher optical gains with downsized active regions. Among them, the oxide confinement structure is the most suitable from the point of view of compatibility of the direct bonding process.

In addition, compared to the proton implantation method, which cannot provide optical confinement between the implanted and un-implanted regions, the oxide confinement structure can realize optical confinement between the oxidized and unoxidized regions. This advantage has been proved by the VCSEL development.[22,25]

Figure 1 shows a hybrid laser structure with AlInAs oxidation layer. A 1-μm-wide waveguide formed on an SOI wafer that consists of a 250-nm top Si layer, 3-μm buried oxide (BOX) layer, and 525-μm Si substrate, is directly bonded with an epitaxially grown InP wafer that includes 5 quantum wells (QWs) of GaInAsP and a 100-nm AlInAs layer. The p-electrode and n-electrode are formed on top of the 7-μm-wide mesa and the bottom n-InP layer, respectively. Figure 2 shows the stripe-width dependence of both threshold current and external differential quantum efficiency, obtained using commercial software PICS3D. It should be noted that the stripe width defined here is the unoxidized width W_s of the AlInAs layer. During the simulation, the cavity length of the hybrid laser is assumed to be 500 μm, with a cleavage facet mirror.

The result indicates that a low threshold current of 5 mA and high external differential quantum efficiency of 30%/facet, which are comparable to that of the conventional III–V-based lasers, can be achieved owing to the volume reduction of the active region with a W_s of approximately 1 μm. $W_s < 1$ μm or $W_s > 2$ μm are not preferred because of the potential escape of the modes into the InP cladding layer or the excitation of higher-order lateral modes. In conclusion, a stripe width W_s of 1–1.5 μm is considered most appropriate for high-efficiency lasing operations.

3. Thermal oxidation process

Two points should be investigated in order to introduce the AlInAs oxidation process into the hybrid laser fabrication

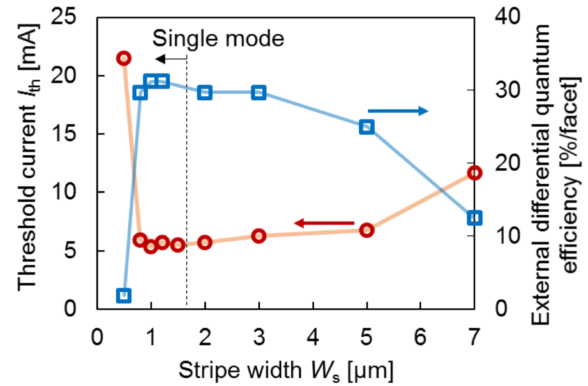

Fig. 2. (Color online) W_s dependence of lasing characteristics.

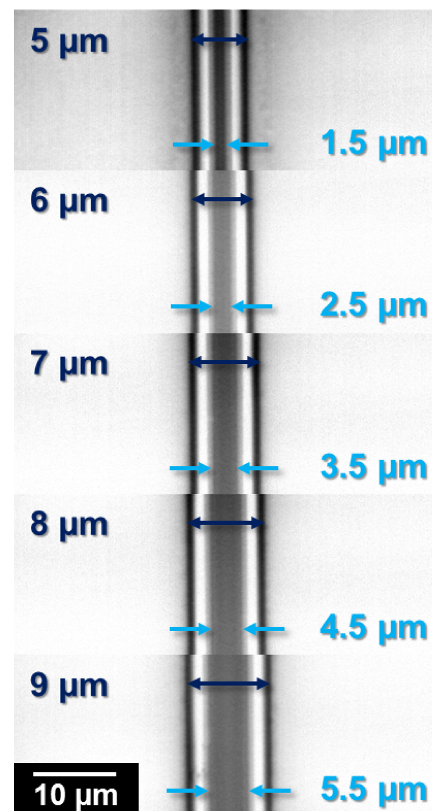

Fig. 3. (Color online) IR microscopic top view of oxidized mesas.

process. One is the oxidation depth of the AlInAs layer. The oxidation rate of the III–V/SOI hybrid wafer depends on the oxidation temperature and the layer thickness. Although it has already been studied before in the case of conventional InP laser structures,[29] it needs to be confirmed for the case of hybrid structures. Another point is the damage to the III–V/SOI wafer caused by the thermal process. Generally, thermal stress is a critical issue for hybrid wafer structures with materials possessing different thermal expansion coefficients, and can cause cracks and removals. Therefore, the assessment of the active layer is conducted by comparing the photoluminescence (PL) spectra before and after oxidation.

First, oxidation is carried out to check the oxidation rate with exactly the same process flow and wafer structure as that of the hybrid laser. Figure 3 shows the IR microscopic top views of the laser mesas after thermal oxidation under the conditions summarized in Table I. Water vapor is produced

 © 2017 The Japan Society of Applied Physics

Table I. Oxidation conditions.

H_2O flow (g/h)	100
N_2 flow (l/min)	20
Rotate speed (rpm)	10
Pretable temp. (°C)	200
Oxidation temp. (°C)	480
Ramp-up time (h)	2
Annealing time (h)	6
Cooling time (h)	2

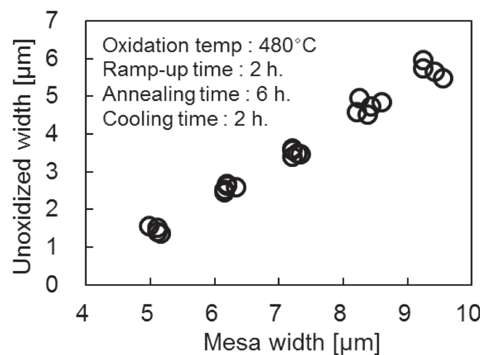

Fig. 4. Mesa-width dependence of unoxidized width.

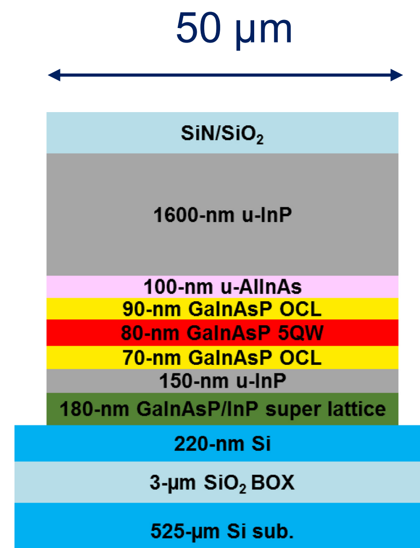

Fig. 5. (Color online) Schematic of layer structure for assessment.

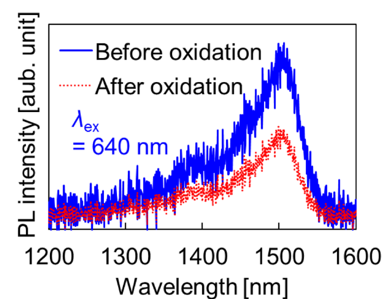

Fig. 6. (Color online) Comparison of PL spectra before and after oxidation ($\lambda_{ex} = 640$ nm).

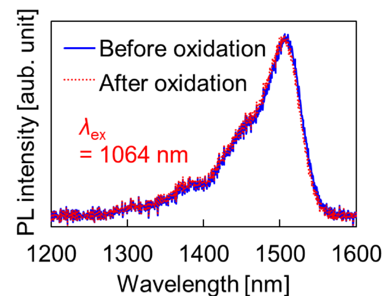

Fig. 7. (Color online) Comparison of PL spectra before and after oxidation ($\lambda_{ex} = 1064$ nm).

by a vaporizer, instead of bubbling, and is introduced to the chamber. The details of the oxidation system can be found in Ref. 30. Figure 4 indicates that an oxidized depth of approximately 2 μm can be obtained by this condition, and that the oxidation rate is approximately 0.3 μm/h, which is independent of the mesa width. This hybrid wafer structure has a slower oxidation rate compared to that in Ref. 25, which used a conventional InP laser structure on an InP substrate.

Next, the wafer damages after both the direct bonding process and the AlInAs oxidation process are investigated. The former had already been reported before,[5)] and it was indicated that a relatively low bonding temperature could provide high bonding strength and had negligible influence on the active region. In this paper, we investigate the latter effect by comparing the PL spectra of the oxidized and unoxidized wafers.

Figure 5 shows the schematic structure of the wafer used in this experiment. The layer structure of the measured wafer is almost the same as that of the hybrid laser, except that each layer is undoped for reducing the carrier absorption. In addition, the GaInAs contact layer, which is required in a real hybrid laser, is omitted during this assessment to eliminate the absorption of PL light from the active layer and the excitation laser light at the GaInAs layer. SiN/SiO_2 dielectric layers are used as a mesa formation mask and protection layer during oxidation. After removing these dielectric layers, the PL characteristics of the wafer are measured using two different excitation lasers with wavelengths of 640 and 1064 nm. For the 1064-nm light, only the GaInAsP optical confinement layers and QWs are excited. In contrast, the 640-nm light excites both QW layers and InP cladding layers.

Figure 6 shows the comparison of the PL spectra at 640 nm, which indicates an obvious degradation in the PL intensity after oxidation. In the case of the 1064-nm excitation light shown in Fig. 7, there appears to be no difference between the PL spectra before and after oxidation, which means that the thermal oxidation process causes negligible damage to the active layers because the 1064-nm light excites only the active layers. Therefore, it is assumed that the degradation of the PL intensity at 640 nm is caused by an absorption of the excitation light due to the thermal decomposition in the InP cladding during the oxidation process at a temperature of 480 °C, which is close to the temperature of InP decomposition. We have confirmed that the PL intensity, even by the 640-nm light excitation, can be recovered after removing several hundred nanometers of the InP layer. Therefore, this issue can be solved in the future by introducing proper protection layers.

 © 2017 The Japan Society of Applied Physics

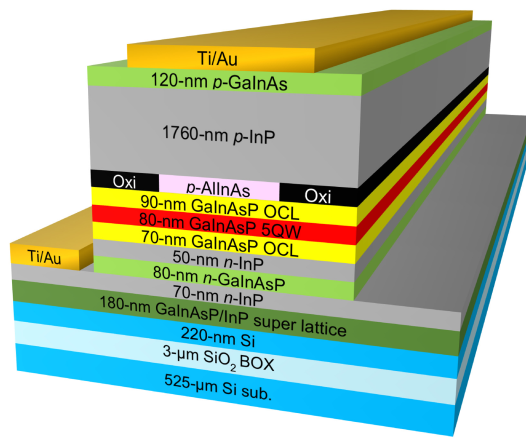

Fig. 8. (Color online) Schematic of a fabricated hybrid laser.

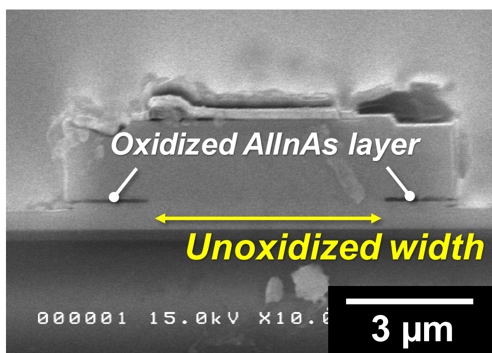

Fig. 9. (Color online) Cross-sectional SEM image of a fabricated hybrid laser.

4. Laser fabrication

Figure 8 shows the schematic of the fabricated hybrid FP laser. First, an epitaxially grown III–V compound semiconductor wafer was bonded on an SOI wafer, using N_2 plasma activated bonding. The III–V compound semiconductor wafer included GaInAsP 5QWs and 100-nm AlInAs layers for the oxide-confinement structure. The active layer consisted of 1% compressively strained $Ga_{0.22}In_{0.78}As_{0.81}P_{0.19}$ wells and 0.15% tensile strained $Ga_{0.26}In_{0.74}As_{0.49}P_{0.51}$ barriers. Please note that the high-performance lasing obtained in the simulation result shown in Fig. 1 may not be achieved since a Si waveguide was not formed on the SOI wafer in the first trial. After the bonding process, the InP substrate and the GaInAs etching stop layer were selectively etched using HCl and H_2SO_4 solutions. SiN and SiO_2 layers were then deposited on the substrate as the dielectric masks used for mesa formation. Next, 5–9-μm stripe mesas were patterned on the dielectric layers by photolithography and transferred onto the III–V compound semiconductor layer by inductive coupling plasma–reactive ion etching with $CH_4/H_2/Cl_2$ mixture gas. After wet treatment with citric acid and ammonia solutions as a preoxidation cleaning, the AlInAs layer was selectively oxidized under the conditions in Table I.

Figure 9 shows the cross-sectional scanning electron microscopy (SEM) image of the fabricated hybrid laser. The oxidation width was observed to be nearly 2 μm from the side wall. A 100-nm-thick SiO_2 insulation layer was

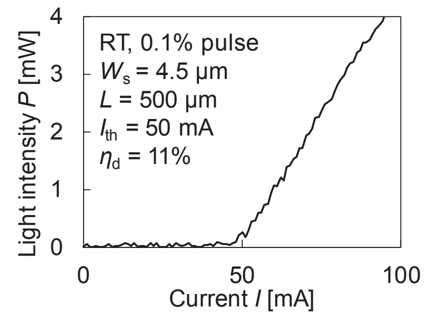

Fig. 10. Lasing characteristics of fabricated laser.

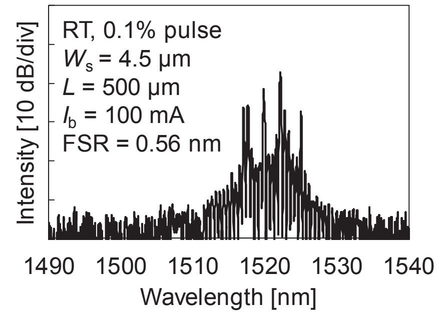

Fig. 11. Lasing spectrum of fabricated laser.

then deposited on the wafer, followed by the patterning of p- and n-type electrodes on the dielectric layer by photolithography. Finally, the contact layers were removed by wet etching and Ti/Au = 25/200 nm were evaporated separately on the p-GaInAs and n-InP layers using an electron beam evaporator.

5. Measurement and discussion

The measured lasing characteristics of the fabricated hybrid laser with a stripe width of 4.5 μm and cavity length of 500 μm at RT pulsed current conditions (1.0-μs pulse width and 0.1% duty cycle) are shown in Fig. 10. A threshold current (I_{th}) of 50 mA and an external differential quantum efficiency of 11%/facet were obtained. Figure 11 shows the lasing spectrum at a bias current of $2I_{th}$. FP modes were observed at approximately 1522 nm with a resonant mode spacing of 0.56 nm. This is the first successful lasing of a III–V/SOI hybrid laser with AlInAs-oxide confinement structure, and it proves the possibility of AlInAs-oxide current confinement structures that require introduction of high-temperature processes into even a different material bonded device. Lasers with $W_s = 4.5$ μm and $L = 500$ μm demonstrated the best performance and highest yield. Lasing operation could not be obtained from devices with unoxidized stripe widths W_s narrower than 3.5 μm because of insufficient optical gain.

Figure 12 shows the cavity-length dependence of the external differential quantum efficiency. An internal quantum efficiency of 39% and an internal loss of 18 cm^{-1} were derived from the linear fitting and theoretical equations. Such low internal quantum efficiencies are assumed to be caused by the unnecessary carrier recombination between the n-type electrode and the active layer, which is considered to be induced by the thermal decomposition that occurred at the n-InP contact layer during the oxidation process. It was

 © 2017 The Japan Society of Applied Physics

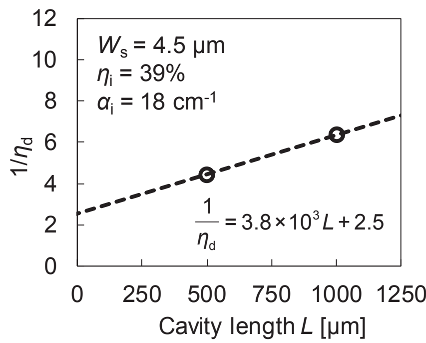

Fig. 12. Cavity-length dependence of the reciprocal of external differential quantum efficiency.

Table II. Parameters used for calculation.

Stripe width W_s (µm)	4.5
Cavity length L (µm)	500
Facet reflectivity R (%)	30
Optical confinement factor ξ (%)	4.7
Active layer thickness d (nm)	6
Internal loss α_i (cm^{-1})	18

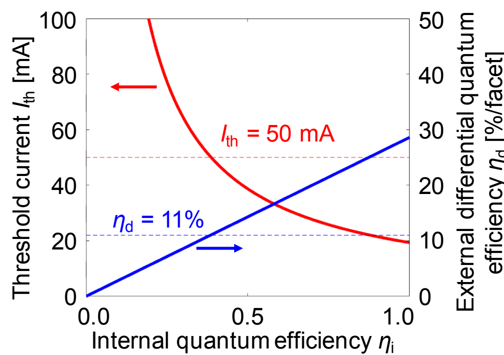

Fig. 13. (Color online) Numerical calculation of internal quantum efficiency dependence of threshold current and external differential quantum efficiency.

experimentally confirmed that a good current path could be formed with a protection layer on the n-type contact layer during the thermal process, as mentioned in Sect. 3. This improvement will provide a higher gain and lower heating, leading to a better lasing condition with narrow W_s and CW operation.

The expected improvement in the lasing conditions based on the increase in the internal quantum efficiency is numerically calculated using the parameters listed in Table II, which include values obtained from the fitting line in Fig. 12. To be specific, the red and blue lines in Fig. 13 indicate the variations in the threshold current and external differential quantum efficiency of the fabricated device shown in Fig. 10, respectively. According to the calculation result, a threshold current of 25 mA and an external differential quantum efficiency of 20%/facet can be expected with an improved internal quantum efficiency from 39 to 80% as a common value in conventional semiconductor lasers. Therefore, protection against thermal decomposition is considered necessary for realizing an efficient III–V/SOI hybrid laser with AlInAs-oxide current-confinement structure.

Based on the investigation of the fabrication process and lasing characteristics, conducted in this paper, we are now working on the improvement of the hybrid FP laser by introducing the AlInAs-oxide confinement structure into a Si-waveguide-integrated hybrid laser.

6. Conclusions

This paper presented the introduction of an AlInAs-oxide confinement structure into a hybrid FP laser, for realizing high-performance III–V/SOI hybrid lasers, which are comparable to the conventional lasers on III–V compound semiconductor wafers. Before the fabrication of the hybrid laser, the influence of the thermal oxidation process on the III–V/SOI bonded wafer was assessed by comparing the PL spectra before and after oxidation. The agreements in the PL spectra of the hybrid wafers excited by the 1064-nm-wavelength light indicated that there would be negligible damage to the active layer. The fabricated III–V/SOI hybrid FP laser with AlInAs-oxide confinement structure had a threshold current of 50 mA and an external differential quantum efficiency of 11%/facet under the RT pulsed current condition. The internal quantum efficiency dependence of the laser characteristic was calculated based on the parameters obtained from the fitting lines. The results showed that a threshold current of 25 mA and an external differential quantum efficiency of 20%/facet could be expected by improving the internal quantum efficiency, which are comparable with the results from other reported hybrid lasers.

Acknowledgments

This work was supported by the New Energy and Industrial Technology Development Organization (NEDO), JSPS KAKENHI Grant Numbers 15H05763, 25709026, 15J11774, and 14J02327, JST-CREST, and JST-ACCEL.

1) Cisco, Visual Networking Index, Forecast and Methodology, 2015–2020.
2) A. Singh, J. Ong, A. Agarwal, G. Anderson, A. Armistead, R. Bannon, S. Boving, G. Desai, B. Felderman, P. Germano, A. Kanagala, J. Provost, J. Simmons, E. Tanda, J. Wanderer, U. Hölzle, S. Stuart, and A. Vahdat, Proc. Conf. Special Interest Group Data Communication, 2015, p. 183.
3) A. Roy, H. Zeng, J. Bagga, G. Porter, and A. C. Snoeren, Proc. Conf. Special Interest Group Data Communication, 2015, p. 123.
4) S. Sezer, S. Scott-Hayward, P. K. Chouhan, B. Fraser, D. Lake, J. Finnegan, N. Viljoen, M. Miller, and N. Rao, IEEE Commun. Mag. **51** [7], 36 (2013).
5) Y. Hayashi, R. Osabe, K. Fukuda, Y. Atsumi, J. H. Kang, N. Nishiyama, and S. Arai, Jpn. J. Appl. Phys. **52**, 060202 (2013).
6) J. Suzuki, Y. Hayashi, Y. Kuno, J. H. Kang, T. Amemiya, N. Nishiyama, and S. Arai, Jpn. J. Appl. Phys. **53**, 118003 (2014).
7) Y. Hayashi, J. Suzuki, S. Inoue, S. M. T. Hasan, Y. Kuno, K. Itoh, T. Amemiya, N. Nishiyama, and S. Arai, Jpn. J. Appl. Phys. **55**, 082701 (2016).
8) K. K. Lee, D. R. Lim, and L. C. Kimerling, Opt. Lett. **26**, 1888 (2001).
9) S. K. Selvaraja, P. D. Heyn, G. Winroth, P. Ong, G. Lepage, C. Cailler, A. Rigny, K. Bourdelle, W. Bogarets, D. Van Thourhout, J. V. Campenhout, and P. Absil, Optical Fiber Communication Conf., 2014, Th2A.33.
10) C. Gunn, IEEE Micro **26** [2], 58 (2006).
11) K. Ogawa, K. Goi, Y. T. Tan, T.-Y. Liow, X. Tu, Q. Fang, G.-Q. Lo, and D.-L. Kwong, Opt. Express **19**, B26 (2011).
12) T. Baba, S. Akiyama, M. Imai, N. Hirayama, H. Takahashi, Y. Noguchi, T. Horikawa, and T. Utsuki, Opt. Express **21**, 11869 (2013).
13) K. Suzuki, K. Tanizawa, T. Matsukawa, G. Cong, S.-H. Kim, S. Suda, M. Ohno, T. Chiba, H. Todokoro, M. Yanagihara, Y. Igarashi, M. Masahara, S. Namiki, and H. Kawashima, Opt. Express **22**, 3887 (2014).
14) T. J. Seok, N. Quack, S. Han, R. S. Muller, and M. C. Wu, J. Lightwave Technol. **34**, 365 (2016).
15) H. Rong, R. Jones, A. Liu, O. Cohen, D. Hak, A. Fang, and M. Paniccia,

© 2017 The Japan Society of Applied Physics

Nature **433**, 725 (2005).
16) Y. Takahashi, Y. Inui, M. Chihara, T. Asano, R. Terawaki, and S. Noda, Nature **498**, 470 (2013).
17) A. W. Fang, H. Park, O. Cohen, R. Jones, M. J. Paniccia, and J. E. Bowers, Opt. Express **14**, 9203 (2006).
18) S. Stankovic, R. Jones, M. N. Sysak, J. M. Heck, G. Roelkens, and D. Van Thourhout, IEEE Photonics Technol. Lett. **23**, 1781 (2011).
19) K. Tanabe, K. Watanabe, and Y. Arakawa, Opt. Express **20**, B315 (2012).
20) C. Zhang, S. Srinivasan, Y. Tang, M. J. R. Heck, M. L. Davenport, and J. E. Bowers, Opt. Express **22**, 10202 (2014).
21) A. Abbasi, J. Verbist, J. V. Kerrebrouck, F. Lelarge, G.-H. Duan, X. Yin, J. Bauwelinck, G. Roelkens, and G. Morthier, Opt. Express **23**, 26479 (2015).
22) D. L. Huffaker, D. G. Deppe, K. Kumar, and T. J. Rogers, Appl. Phys. Lett. **65**, 97 (1994).
23) N. Ohnoki, N. Hatori, A. Mizutani, F. Koyama, and K. Iga, Jpn. J. Appl. Phys. **36**, 1896 (1997).
24) N. Iwai, T. Mukaihara, N. Yamanaka, K. Kumada, H. Shimizu, and A. Kasukawa, IEEE J. Sel. Top. Quantum Electron. **5**, 694 (1999).
25) Y. Hayashi, T. Mukaihara, N. Hatori, N. Ohnoki, A. Matsutani, F. Koyama, and K. Iga, Electron. Lett. **31**, 560 (1995).
26) Y. Takino, M. Shirao, T. Sato, N. Nishiyama, T. Amemiya, and S. Arai, Jpn. J. Appl. Phys. **50**, 070203 (2011).
27) S. M. Ullah, R. Suemitsu, S. H. Lee, M. Otake, N. Nishiyama, and S. Arai, Jpn. J. Appl. Phys. **46**, L1068 (2007).
28) D. Inoue, J. Lee, K. Doi, T. Hiratani, Y. Atsuji, T. Amemiya, N. Nishiyama, and S. Arai, Appl. Phys. Express **7**, 072701 (2014).
29) N. Iwai, T. Mukaihara, M. Itoh, N. Yamanaka, S. Arakawa, H. Shimizu, and A. Kasukawa, LEOS '98, 1998, p. 118.
30) M. Arai, N. Nishiyama, S. Shinada, F. Koyama, and K. Iga, Jpn. J. Appl. Phys. **39**, 3468 (2000).

 © 2017 The Japan Society of Applied Physics